

Heat flow map and geothermal resources in Mexico[☆]

Mapa de flujo de calor y recursos geotérmicos de México

Rosa-Maria Prol-Ledesma^a, Juan-Luis Carrillo-de la Cruz^b, Marco-Antonio Torres-Vera^b, Alejandra-Selene Membrillo-Abad^b, Orlando-Miguel Espinoza-Ojeda^c

^a*Instituto de Geofísica, Universidad Nacional Autónoma de México, Cd. Universitaria, Cd. De México, CP 04510, México.*

^b*Posgrado en Ciencias de la Tierra, Instituto de Geofísica, Universidad Nacional Autónoma de México, Cd. Universitaria, Cd. De México, CP 04510, México.*

^c*CONACyT - INICIT, Universidad Michoacana de San Nicolás de Hidalgo, Morelia, Michoacán, CP 58060, México*

Abstract

Heat flow maps are a powerful tool for regional exploration of geothermal resources. Mexico is one of the main producers of geothermal energy and the search for undiscovered resources at a regional level should be based on heat flow values. Here, we present a heat flow map at 1:3,500,000 scale, produced with heat flow data compiled from open data bases and previously unpublished data. The compiled heat flow data includes bottom hole temperature, temperature logs, transient temperature measurements and measured temperature logs. The new data were calculated from temperature gradient information and estimating a mean conductivity value characteristic for the type of rock present in the stratigraphic column or assigning the mean conductivity value for the crust. Geothermal gradient and the thermal resistivity (inverse thermal conductivity) were plotted and heat flow was calculated using the Bullard method. The map covers the whole continental territory of Mexico and shows that most of the country has values higher than the world average. The highest heat flow values are concentrated in two provinces: the Gulf of California extensional province and the Trans-Mexican Volcanic Belt.

Keywords: Geothermal; recent volcanism; renewable energy, geothermal gradient, Bullard method, BHT

Resumen

Los mapas de flujo de calor son una poderosa herramienta en la exploración regional de recursos geotérmicos. México es uno de los principales productores de energía geotérmica y la búsqueda a nivel regional para descubrir nuevos recursos debería estar basada en los datos de flujo de calor. Aquí presentamos el mapa de flujo de calor a escala 1:3,500,000, que fue generado a partir de datos de flujo de calor compilados en bases de datos públicas, a los cuales se añadieron nuevos datos calculados por los autores. Los datos compilados para el cálculo del mapa de flujo de calor incluyen: temperatura de fondo de pozo (BHT), registros de temperatura en pozos (compilados y medidos en este trabajo), mediciones transientes de temperatura. Los datos que no han sido reportados previamente fueron calculados a partir de la determinación del gradiente de temperatura y la estimación de la conductividad térmica promedio para los tipos de roca reportados en la columna estratigráfica, o bien, en ausencia de la información acerca del tipo de roca, se asignó el valor promedio de la conductividad para la corteza. El gradiente geotérmico y la resistividad térmica (el inverso de la conductividad térmica) se graficaron para determinar el flujo de calor con el método de Bullard. El mapa cubre todo el territorio continental mexicano y muestra que en la mayor parte los valores de flujo de calor están por encima del flujo de calor promedio a nivel mundial. Los valores más altos de flujo de calor se concentran en la provincia extensional del Golfo de California y en la Faja Volcánica Trans-Mexicana.

Palabras clave: Geotermia; volcanismo reciente; energía renovable, gradiente geotérmico, método de Bullard, BHT

[☆] © R. M. Prol-Ledesma, J. L. Carrillo-de la Cruz, M. A. Torres-Vera, A. S. Membrillo-Abad and O. M. Espinoza-Ojeda. Published by Terra Digitalis. This is an Open Access article distributed under the terms of the Creative Commons Attribution License (<https://creativecommons.org/licenses/by-nc-sa/4.0/>),

which permits non-commercial sharing of the work and adaptions, provided the original work is properly cited and the new creations are licensed under identical terms.

*E-mail address: prol@unam.mx

1. Introduction

The total heat flux through the Earth's surface has been quantified at 47 ± 2 TW (Davies & Davies, 2010); while in 2017, the reported installed capacity in the world to produce electricity was a little more than 6 TW (<https://www.cia.gov/library/publications/the-world-factbook/rankorder/2236rank.html>). This shows that the energy irradiated by the Earth's surface is almost 8 times the world installed capacity for electricity generation and could be harnessed to supply, at least a part of the world energy needs.

The surface heat flow is an indication of the transport of heat from the interior of the Earth and its value depends greatly on the transport mechanism as well as the heat production in the crust. In most of the crust, heat is transported conductively; however, in some areas the more efficient convective heat transport predominates. To have convection in the crust, a fluid must be allowed to ascend to the surface carrying the heat in the upper crust, this fluid is often water, but magma is the dominant fluid for heat transport from the lower crust and from the mantle. The hot water can be used to produce electricity, for climatization and industrial processes.

The evaluation of the geothermal potential of a country is often linked to a heat flow map (White & Williams, 1975; Muffler & Cataldi, 1978; Muffler, 1979; Blackwell et al., 2007; van Wees et al., 2013). Heat flow values delineate the areas where the temperature at depth potentially allows exploitation of the thermal energy with the available technology. Temperatures at depth can be calculated assuming a conductive model; in this case, it is necessary to know the value of the thermal conductivity of the rocks and its chemistry to estimate the heat production by the radioactive element content. Recent tectonic and volcanic activity plays a major role in the heat flow values; heat transport models show that the maximum value of heat flow, due to an igneous intrusion in the crust, is attained after 100,000 years if convection occurs, and when conduction prevails, heat flow would decrease exponentially one order of magnitude in $\sim 200,000$ years (Norton & Knight, 1977). Therefore, a heat flow map may provide evidence about the presence of heat sources based on heat transport models.

2. Heat flow data

Heat flow measurements are scarce in Mexico, despite being one of the ten countries with the highest electricity production from geothermal energy. Published heat flow maps of the region included data calculated with temperature measurements in wells (Blackwell & Richards, 2004) but most of the heat flow reports were based on estimations, using diverse methods (Marvin, 1984; Prol-Ledesma & Juárez, 1986; Campos-Enriquez et al., 1990; Prol-Ledesma, 1990, 1991b; Beltrán-Abaunza & Quintanilla-Montoya, 2001; Prol-Ledesma & Torres-Vera, 2007; Espinosa-Cerdeña & Campos-Enríquez, 2008; Manea & Manea, 2010). Heat flow estimations are generally based on silica geothermometer, Curie Temperature Depth, and Helium isotopic

ratio (${}^3\text{He}/{}^4\text{He}$) (Swanberg & Morgan, 1978; Okubo, 1985; Poljak, 2005). More recent estimations have included geological and geophysical information (Goutorbe et al., 2011).

The heat flow map presented in this work was constructed using only data calculated with temperatures measured in wells because other estimations are less reliable. In fact, silica concentration in spring/well water is indicative of temperature at depth, provided chemical equilibrium is attained, which is not always the case. Furthermore, a parameter that remains unknown is the equilibrium depth, which hinders an accurate calculation of thermal gradient. The relation between silica geothermometer and heat flow is only qualitative, the correlation coefficient is $<50\%$ (Fig. 1) and should not be used as an exact determination to be included in thermal models.

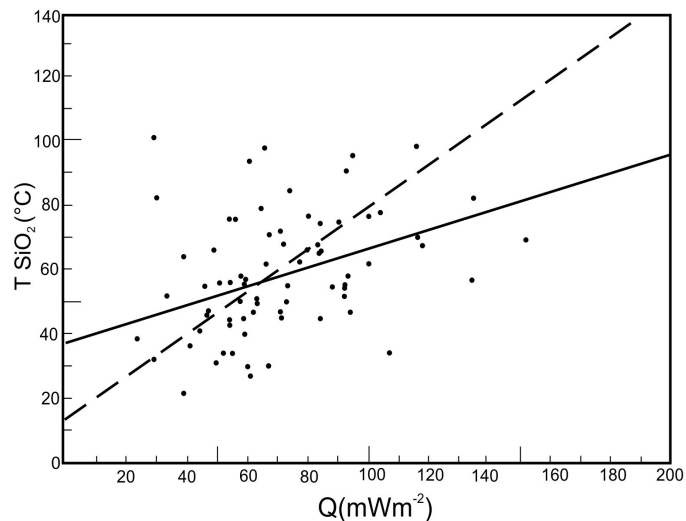


Figure 1. Plot of silica temperature vs heat flow
(Modified from Swanberg & Morgan, 1980).

Figura 1. Temperatura de sílice contra flujo de calor.

Similar ambiguity is present in heat flow estimations using the ${}^3\text{He}/{}^4\text{He}$ and Curie temperature depth (CTD). The comparison between measured heat flow and estimations calculated from CTD show significant differences in some areas (e.g. Manea & Manea, 2010). According to Bouligand et al. (2009), discrepancies between heat flow and calculated CTD arise when thermal conductivities and/or heat generation are not well constrained; additionally, 3-D variations in thermal conductivity, rapid erosion or sedimentation, variations on radioactive heat production, heat provided by recent volcanism or groundwater circulation may cause large discrepancies. More importantly, in some cases the bottom of the magnetic sources may be a lithologic contact corresponding to the base of the crust and not the actual CTD; additionally, there might be artifacts associated to the acquisition of the data. In the classic paper on CTD, Okubo (1985) did not intend to calculate heat flow, but to produce a qualitative relation between shallow CTD and the occurrence of geothermal systems; further comparison of calculated CTD with geothermal gradient measurements produced signif-

ificant inconsistencies (Okubo et al., 1989). These discrepancies are also present in the estimation of the geothermal gradient of Cerro Prieto using CTD, yielding values ranging between 33 and 38 °C/km and a heat flow of 100 mW/m² (Espinosa-Cerdeña & Campos-Enríquez, 2008); while the reported well temperature (Lippmann et al., 1991) indicates a gradient higher than 100 °C/km.

The relation between heat flow and ³He/⁴He is based on the assumption that high ³He/⁴He is caused by mantle upwelling and degassing that would produce high heat flow anomalies (Polyak, 1985; Polyak & Tolstikhin, 1985; Polyak, 2005); however, the scattered data prevents a reliable quantitative correlation between both parameters (Fig. 2).

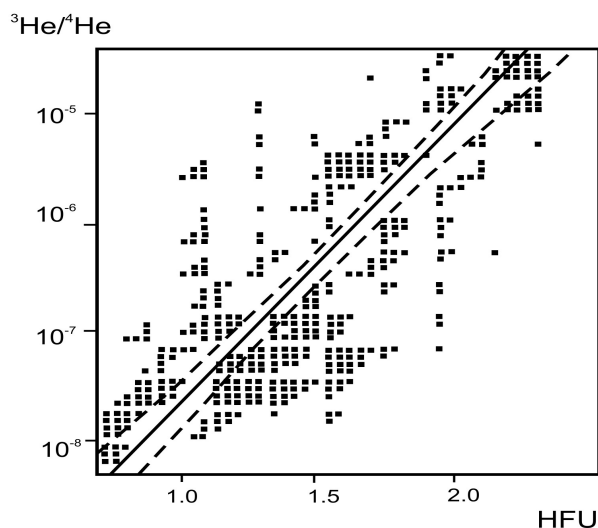


Figure 2. Plot of ³He/⁴He vs heat flow that shows the large scatter of the data. It also shows the best correlation between both parameters that would support calculation of heat flow with the isotopic helium ratio (after Polyak, 2005). Figura 2. ³He/⁴He contra flujo de calor mostrando la gran dispersión de los datos. También muestra la mejor correlación entre ambos parámetros, la cual soportaría el cálculo del flujo de calor a partir del cociente ³He/⁴He.

At the beginning of the XXI century, the heat flow measurements reported in the continental part of Mexico (Smith, 1974; Smith et al., 1979; Reiter & Tovar, 1982; Ziagos et al., 1985; Flores-Márquez et al., 1999) were more scarce than those in the ocean bottom, where more than 700 heat flow measurements were published (Becker & Fisher, 1991; Epp et al., 1970; Fisher et al., 2001; Khutorskoy et al., 1990; Lawver & Williams, 1979; Nagihara et al., 1996; Prol-Ledesma et al., 1989; Vacquier et al., 1967; Von Herzen, 1963; Von Herzen & Uyeda, 1963). However, since the creation of the Mexican Center for Innovation in Geothermal Energy (CeMIE-Geo), a great effort has been made to compile and produce more heat flow data and construct a reliable heat flow map to assist the evaluation of the geothermal potential of the country (Espinoza-Ojeda et al., 2017 a,b; Neumann et al., 2017; Prol-Ledesma et al., 2013; Prol-Ledesma et al., 2016; Prol-Ledesma, 2018). The compilation of all available data to calculate the geothermal gradient and the measurement of temperature in wells, produced a large increase in the

number of data. Heat flow data assembled for this work are available in public data bases: Heat Flow Database (<http://www.datapages.com/gis-map-publishing-program/gis-open-files/global-framework/global-heat-flow-database>), Pangea database (<https://doi.pangaea.de/10.1594/PANGAEA.810104>), the International Heat Flow Commission [IHFC] (<http://engineering.und.edu/geology-and-geological-engineering/globe-heat-flow-data-base/index.cfm>), and the SMU Geothermal Lab database (<https://www.smu.edu/Dedman/Academics/Programs/GeothermalLab/DataMaps>).

Additionally, temperature data in wells were measured by our group to calculate heat flow using estimated values for thermal conductivity. In other cases we obtained drilling information for some previously reported data that allowed recalculating the borehole stable temperature (Appendix Table 1). When the temperature logs were available, the data were reviewed and analyzed; in some cases, they were reprocessed to calculate the borehole stable temperature and the heat flow based on the Bullard Method. In all cases the confidence of the data was estimated. The data were discarded when the correlation coefficient obtained by the Bullard Method was lower than 90%. A table of the recalculated and previously unreported data used in the map is included as supplemental online material with references to the original publications (Appendix Table 1). Here, we present the map produced by the interpolation of all heat flow data (Plate 1). The interpolation was achieved using the methodology described in this work. This map represents all heat flow data in Mexico available to date and it will be continually updated.

3. Tectonic Framework

The tectonic structure of Mexico is quite complex, as it is formed of diverse terranes (Campa & Coney, 1983; Sedlock et al., 1993), many of them allochthonous, whose relations are obscured by the widely distributed Cenozoic volcanic products (Morán-Zenteno, 1986). It is precisely the widely spread Cenozoic volcanic-tectonic activity that determines the thermal regime of most geological provinces, especially the Neogene and Quaternary volcanism (Morán-Zenteno et al., 2007). This activity is better related to the physiographic provinces (Fig. 3) than to the tectono-stratigraphic terrains, and the numerous surface hydrothermal manifestations are evidence of the extensive thermal anomalies (Appendix Figure 1). Figure 3 includes recent (<3 My) volcanism because the current models used for geothermal exploration (Moeck & Beardmore, 2014) consider that one of the geological settings for “viable” or “active” geothermal systems may be related to igneous activity with age <3 My (Pleistocene and Holocene volcanism in <https://volcano.si.edu/>, intraplate volcanism in Aranda-Gómez et al., 2005; Ferrari et al., 2005, 2007; Vidal-Solano et al., 2005).

The main Cenozoic geodynamic events (Fig. 3) are the subduction of the Farallon Plate in western Mexico, the cessation of subduction after the approaching of the oceanic ridge with

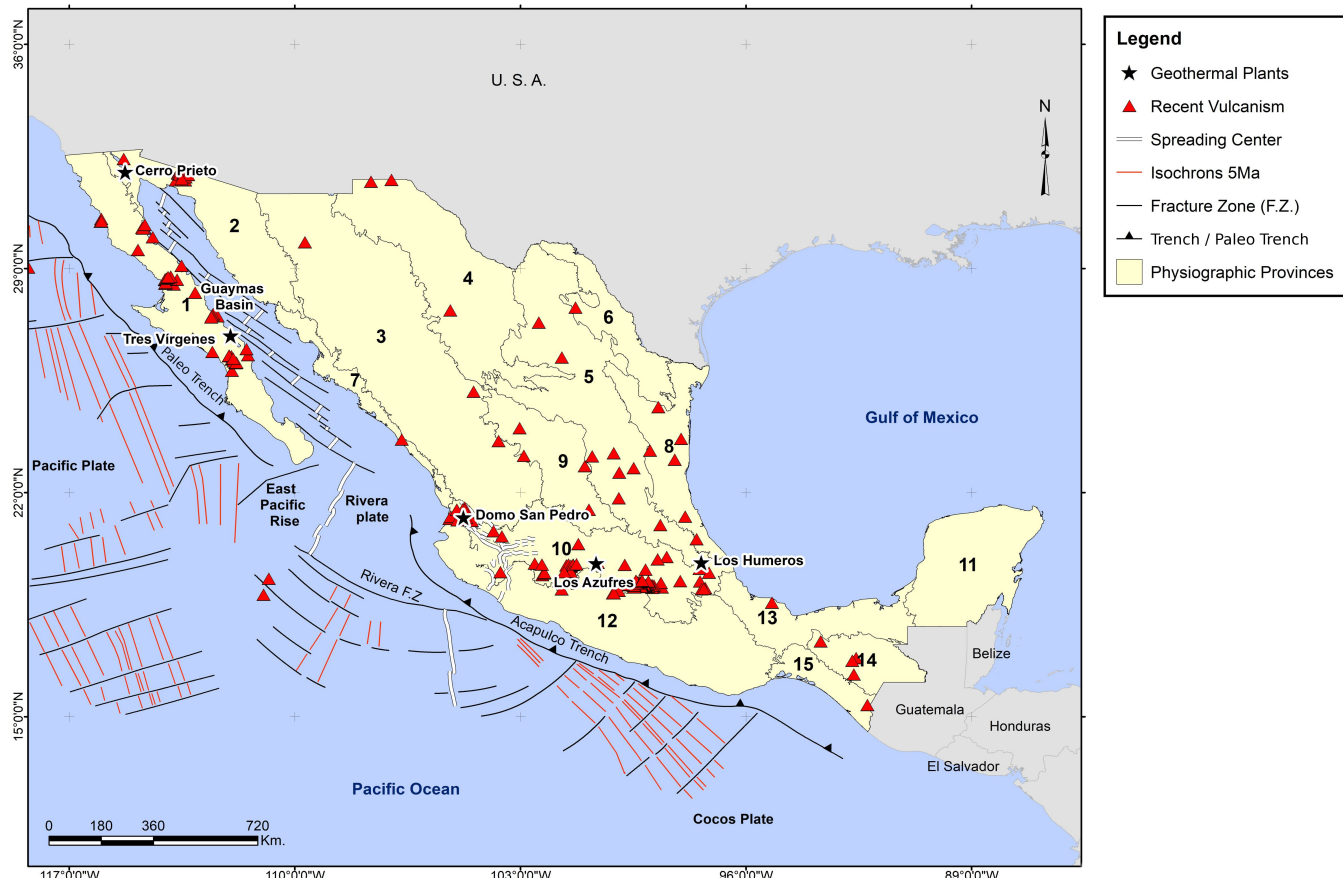


Figure 3. Main morpho-tectonic features of the pacific oceanic floor (modified after INEGI, 2001 and Padilla, 2013). The distribution of physiographic provinces of México and volcanic features < 3 My are also shown. 1. Baja California Peninsula; 2. Sonora Plains; 3. Sierra Madre Occidental; 4. Basin and range province; 5. Sierra Madre Oriental; 6. North America Plains; 7. Pacific Coastal Plains; 8. Gulf of Mexico coastal plains-north ; 9. Mesa Central Province; 10. Mexican Volcanic Belt; 11. Yucatán Peninsula; 12. Sierra Madre del Sur; 13. Gulf of Mexico coastal plains-south; 14. Sierra de Chiapas – Guatemala; 15. Central America Volcanic Belt. Volcanism with age < 3My after: <https://volcano.si.edu/>; intraplate volcanism after Aranda-Gómez et al., 2005; Ferrari et al., 2005, 2007; Vidal-Solano et al., 2005.

Figura 3. Rasgos morfotectónicos del piso oceánico del Pacífico. Distribución de las provincias fisiográficas en México y centros volcánicos de < 3 Ma. 1. Península de Baja California; 2. Planicie de Sonora; 3. Sierra Madre Occidental; 4. Provincia de cuencas y sierras; 5. Sierra Madre Oriental; 6. Planicie de Noreste América; 7. Planicie de la Costa del Pacífico; 8. Planicie al norte del Golfo de México; 9. Provincia de la Mesa Central; 10. Cinturón Volcánico Mexicano; 11. Península de Yucatán; 12. Sierra Madre del Sur; 13. Planicie al sur del Golfo de México; 14. Sierra de Chiapas – Guatemala; 15. Cinturón Volcánico de Centro América.

the trench and the extensional regime associated with these processes that culminate in the opening of the Gulf of California. On the other hand, subduction of the Rivera and the Cocos Plates continues beneath the central and south-western part of Mexico (Atwater, 1970). These events produced geologic provinces like the Sierra Madre Occidental, the Trans-Mexican Volcanic Belt and the formation of the continental rift, locally evolved to ocean spreading, in the Gulf of California. The Cerro Prieto geothermal field is linked to this latter geodynamic process (Fig. 3). Extensional tectonics is also observed in the western part of Mexico, where a late Cenozoic rift triple junction (Jalisco Triple Junction) delineates the Jalisco Block. These rifts are associated with Plio-Quaternary alkaline and peralka-

line volcanics, typical of continental rifting processes (Allan et al., 1991). An interesting feature in the west-central part of southern Mexico, is the Orozco Fracture Zone (OFZ) that is subducted below the Tzitzio Gap (Blatter and Hammersley, 2010), where some hydrothermal systems have been recently reported (Jácome-Paz et al., 2018). In addition to the extensional tectonics in the Gulf of California and subduction in southwestern Mexico, intraplate-type volcanism, often associated with normal faulting (late Oligocene-Quaternary), is widespread in the northern and central parts of Mexico (Aranda-Gómez et al., 2005) and to the east in the Gulf of Mexico coast (Ferrari et al., 2005). Heat flow positive anomalies appear to be linked to this type of volcanism.

4. Methodology

4.1. Heat flow calculation

Heat flow is calculated using the Fourier equation that assumes conductive heat transport:

$$q = -k(dT/dz) \quad (1)$$

where q -heat flow; k -thermal conductivity; T -temperature and z -depth. Available temperature gradient information was analyzed for data screening of geothermal gradient data. This screening was performed to remove local convective effects, especially for those measurements located within hydrothermal systems, to determine the superficial regional conductive heat flow. This was achieved by analyzing the Bullard plots to establish the linear regression between thermal resistance and temperature gradient:

$$T_d = T_o + q_o R \quad (2)$$

where T_d is temperature at depth, T_o is the temperature at surface, q_o is the surface heat flow and R is thermal resistance expressed as:

$$R = \sum_i \left(\frac{\Delta z_i}{k_i} \right) \quad (3)$$

where k_i is the thermal conductivity over the i -th stratigraphic interval at depth and Δz_i is the thickness of the interval.

As an example, Figure 4a shows temperature increases linearly with depth for well MEX060; this linear relationship is preserved in the dependence between the temperature and thermal resistance in the Bullard plot of Figure 4b.

On the other hand, Figures 4c and 4d show temperature plots for well MEX023; high resolution temperature logs are

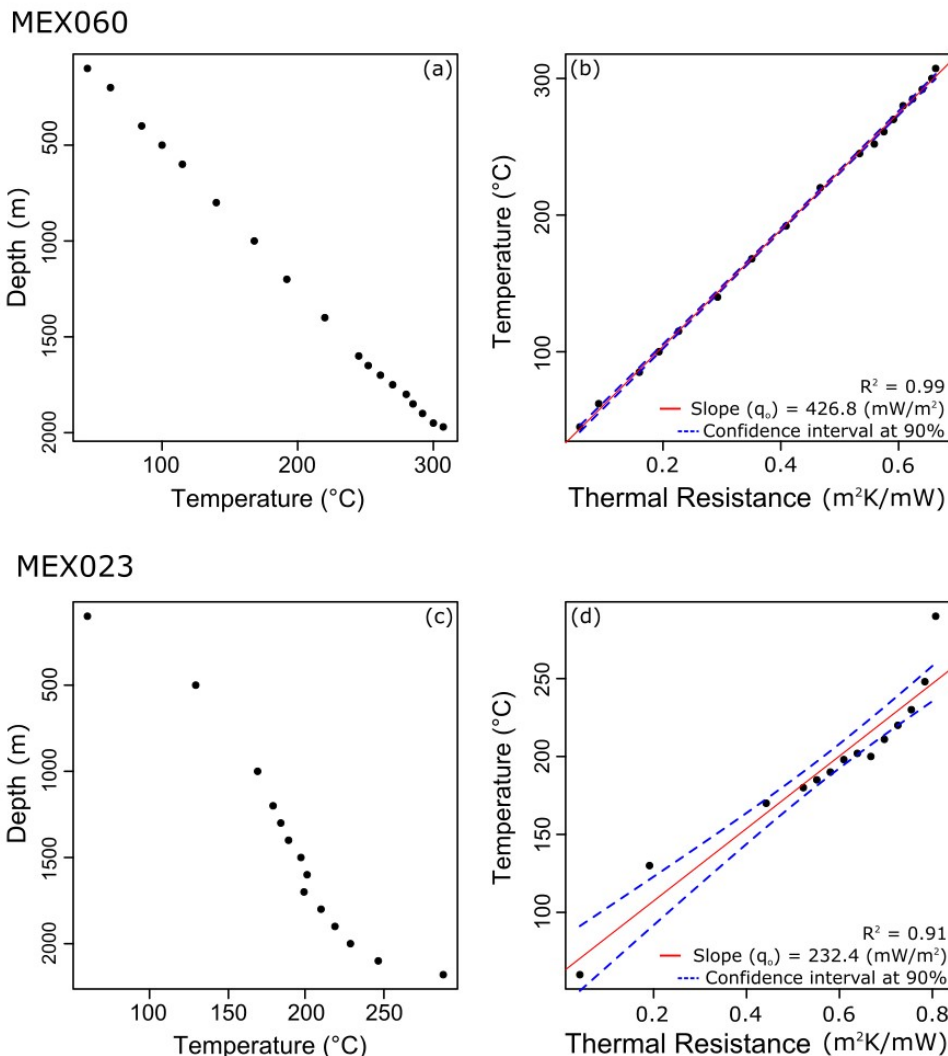


Figure 4. a) Temperature-depth profile and b) Bullard Plot from well MEX060. c) Temperature-depth profile and d) Bullard Plot from well MEX023.
Figura 4. a) Perfil temperatura-profundidad y b) Gráfico Bullard del pozo MEX060. c) Perfil temperatura-profundidad y d) Gráfico Bullard del pozo MEX023.

very useful to identify disturbances in the conductive regime within the well, but the Bullard plot allows to estimate heat flow and the confidence of the slope determination.

The well data used to calculate heat flow by the Bullard Method satisfy parameters of reliability proposed by Richards et al. (2012). Some of these parameters are: (1) the “normal” gradient conditions may be found below 200 meters depth, and (2) multiple gradient intervals are assigned to thermal conductivity values using a weighted average.

The error in the presented new heat flow data can be calculated from the correlation coefficient for each well. A well disturbed by a convection flow has a low correlation coefficient. Accordingly, disturbed wells with a correlation coefficient below 90% were discarded. Only undisturbed wells with a coefficient correlation above 90% were considered for the construction of the map. Disturbed data are easy to identify in high resolution temperature logs using a gradient-depth plot. However, wells with few data are more difficult to analyze for identification of convection disturbances (Beck & Balling, 1988; Cull & Sparksman, 1977); therefore, wells with few data and low correlation coefficients were discarded. All new heat flow data included in the Appendix Table 1, have an accuracy of more than 90% with a positional accuracy of $\pm 50\text{m}$.

4.2. Interpolation

The interpolation was performed using the Inverse Distance Weighting algorithm (IDW). IDW estimates an unknown value of z at location u as a weighted average of its surrounding points, in which the weight is the inverse of the distance raised to a power, according to Tobler’s first law of geography (Chang, 2004; Wang, 2006). The observations of z at points closer to u have a higher weight in the interpolation than those at a greater distance (Brunsdon & Comber, 2015).

The algorithm is defined as:

$$z_u = \frac{\sum_{i=1}^s z_i d_{ui}^{-k}}{\sum_{i=1}^s d_{ui}^{-k}} \quad (4)$$

where:

- z_u is the unknown heat flow value to be estimated at location u .
- z_i is the heat flow value at control point i .
- d_{ui} is the distance between points i and u .
- s is the number of points used in the calculation
- k is the power the distance is raised to.

In the IDW algorithm, the power controls the weight function decrease rate with increasing distance (Bonham-Carter, 1994).

IDW is used in Earth Sciences when the data set does not present a smooth variation but contains large anomalies (Sestianto & Triandini, 2013). Other methods, like Kriging, smooth the interpolated values and the anomalies are discarded. In exploration work, the anomalies are frequently the target for the

discovery of natural resources (Shepard, 1968), as is the case in geothermal exploration; therefore, the selection of the IDW method agrees with the purpose of the map (Plate 1).

4.3. Evaluation of the error in the interpolation process

The evaluation of the error utilized the mean squared error (MSE) method to assess the differences between the actual heat flow measurements and the estimation calculated with the interpolation. The plot that represents the actual heat flow values and the associated interpolated value is shown in Figure 5.

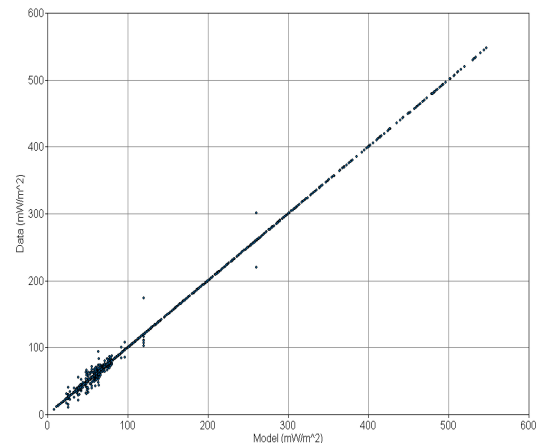


Figure 5. Error plot. The actual heat flow data values are plotted vs the modelled values in the simulation. See text for details.

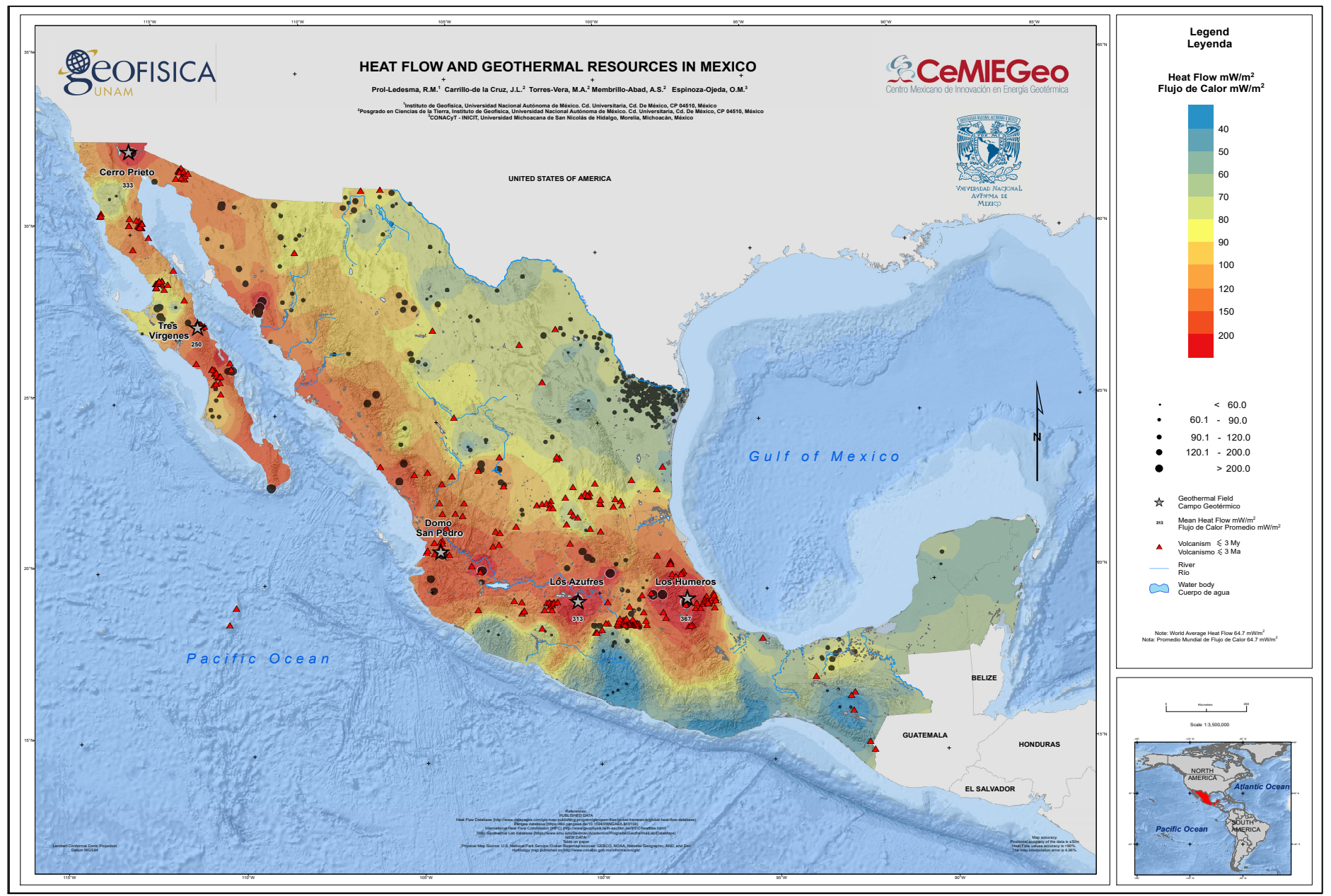
Figura 5. Gráfico de error. Los valores reales de flujo de calor están graficados contra los valores de la simulación. Ver texto para detalles.

These values were used to calculate the MSE that yields a value of 4.96% for the map, which validates the interpolation process. Figure 6 represents the error obtained for all points in the map.

5. Map Synopsis

The interpolation of all the available heat flow measurements for the continental region of Mexico indicates that high heat flow is prevalent in extensive areas in Mexico, and prospective zones are found outside of the active Mexican Volcanic Belt, where so far, most exploration work has been carried out. Three geothermal fields have been developed within the Mexican Volcanic Belt and two in the Baja California Peninsula (Fig. 3 and Plate 1). However, large areas with heat flow at least twice the world mean value have not been explored yet.

The map shows a correlation between high heat flow and recent thermal events related with volcanic-tectonic activity especially in the western and central parts of Mexico, where active subduction, sea floor spreading, and continental rifting is taking place; however, new regions where no exploration campaigns have taken place are pointed out in the map as future targets.



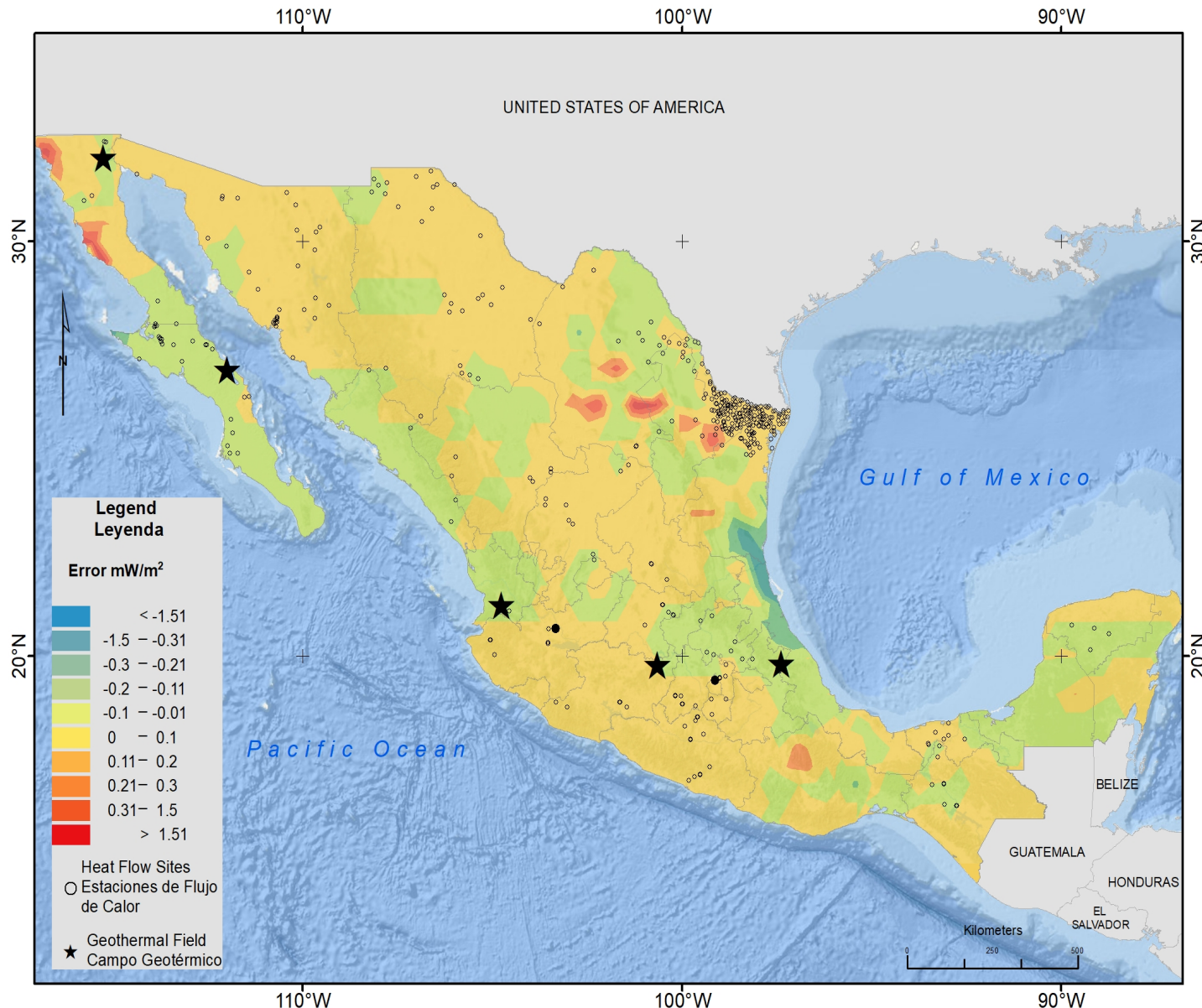


Figure 6: Map showing the error of heat flow interpolated values.
Figure 6. Mapa del error en los valores interpolados de flujo de calor.

The average heat flow for continents is $64.7 \text{ mW}\cdot\text{m}^{-2}$ (Davies, 2013), and a large part of Mexico presents heat flow values over $100 \text{ mW}\cdot\text{m}^{-2}$. This fact suggests that Mexico's geothermal potential has not been exhausted yet and that more intense exploration should be pursued in the newly appointed areas. In contrast, heat flow values, as low as $13 \text{ mW}\cdot\text{m}^{-2}$, have been measured in the Pacific coast region as a result of subduction of the oceanic plate (Zigogos et al., 1985); these areas are characterized by a deep Curie isotherm, between 16 and 24 km (Manea & Manea, 2010).

The Baja California Peninsula exhibits large areas with high heat flow above $100 \text{ mW}\cdot\text{m}^{-2}$. Two geothermal fields are currently under exploitation (Fig. 3 and Plate 1) but regional exploration indicates that the geothermal energy potential may be above 400 MWe (Arango-Galván et al., 2015), and the heat flow map confirms that large resources occur in this region. Heat flow is high along the eastern coast of the Gulf of California as evidence of the sea floor spreading processes taking place nearby.

The eastern part of central Mexico stands out with heat flow values above $150 \text{ mW}\cdot\text{m}^{-2}$. Part of this area corresponds to the limits of the Trans-Mexican Volcanic Belt, but the northern and southern sections are related to high thermal gradients within the oil fields, in some wells the thermal gradient is above $50-70 \text{ }^{\circ}\text{C}/\text{km}$ (Eguiluz-de Antuñano, 2009).

The Sierra Madre Occidental and the intraplate recent volcanic features in the central and eastern parts of Mexico represent the least studied high heat flow anomalies in Mexico (Prol-Ledesma, 2018), and a possible target for future geothermal exploration.

The southeastern part of Mexico contains the oldest provinces as the Oaxaca Terrain (Campa & Coney, 1983) and at the same time it hosts active volcanoes: El Chichón and Tacana; the heat flow measurements have been performed in areas with predominance of the old terrains thermal regime where low heat flow values predominate; nevertheless, high heat flow data in the northern part of this area influence nearby zones as evidence of hotter than average areas.

6. Conclusions

The heat flow values indicate that a large part of Mexico contains promising areas for exploitation and direct utilization of geothermal energy. The most important result is that geothermal exploration should be continued in a regional basis focused on the heat flow anomalies revealed by this map.

The heat flow map will be indispensable for the definition of the geothermal provinces of Mexico, which will guide exploration in the future to fully develop the geothermal resources. Undoubtedly, the future increase in heat flow measurements is necessary and will reveal major high heat flow anomalies in large areas that remain uncharted.

7. Software

We developed our own programs to calculate the well stable temperature and to apply the Bullard method used to compute the new heat flow data. The interpolation process was performed with the IDW algorithm in ESRI ArcGIS.

8. Map Design

The coordinate system used for the map is WGS 84 (World Geodetic System 1984) that locates sites by Latitude, Longitude and Elevation. In this map we will use only Lat/Long to locate the heat flow sites. Geographic coordinates can be used for the whole country without much distortion. We used shape files of Countries from Wessel & Smith (2017). We used the ArcMap platform for administration of geographic data.

- Scale 1:3,500,000 and interpolation was performed in A0.
- Map is oriented to the geographic north
- The total area is $1,881,032 \text{ Km}^2$
- Grade spacing: $5^{\circ}0'0.0''$

Acknowledgements

The authors wish to thank J. Miguel Flores Velazquez, Marcela Errasti-Orozco, Claudia Arango, José Luis Salas, Xóchitl Flores and Juan Antonio Tapia for their help in collecting and processing the data. This work was supported by Fondo de Sustentabilidad Energética SENER-CONACyT CeMIE-Geo under Grant-Project P-01: Mapas de Gradiente Geotérmico y Flujo de Calor para la República Mexicana". The authors thank the comments by two anonymous reviewers that greatly improve the original manuscript.

References

- Allan, J. F., Nelson, S. A., Luhr, J. F., Carmichael, I. S. E., Wopat, M., Wallace, P. J., 1991. Pliocene-Holocene Rifting and Associated Volcanism in Southwest Mexico: An Exotic Terrane in the Making: Chapter 21: Part III. Regional Geophysics and Geology 114, 425–445, doi:10.1306/M47542C21.
- Aranda-Gómez, J. J., Luhr, J. F., Housh, T. B., Valdez-Moreno, G., Chávez-Cabello, G., Aranda-Gómez, J. J., Luhr, J. F., Housh, T. B., Valdez-Moreno, G., Chávez-Cabello, G., 2005. El volcanismo tipo intraplaca del Cenozoico tardío en el centro y norte de México: una revisión. Boletín de la Sociedad Geológica Mexicana 57 (3), 187–225, doi:10.18268/bsgm2005v57n3a1.
- Arango-Galván, C., Prol-Ledesma, R. M., Torres-Vera, M. A., 2015. Geothermal prospects in the Baja California Peninsula. Geothermics 55, 39–57, doi:10.1016/j.geothermics.2015.01.005.
- Atwater, T., Dec. 1970. Implications of Plate Tectonics for the Cenozoic Tectonic Evolution of Western North America. GSA Bulletin 81 (12), 3513–3536, doi:10.1130/0016-7606(1970)81[3513:IOPTFT]2.0.CO;2.
- Beck, A. E., Balling, N., 1988. Determination of Virgin Rock Temperatures. Solid Earth Sciences Library. Springer Netherlands, Dordrecht, doi:10.1007/978-94-009-2847-3_3.
- Becker, K., Fisher, A. T., 1991. A Brief Review of Heat-Flow Studies in the Guaymas Basin, Gulf of California: Chapter 33: Part VI. Hydrothermal Processes. American Association of Petroleum Geologist Memoir 47, 709–720.

- Beltrán-Abaunza, J. M., Quintanilla-Montoya, A. L., Mar. 2001. Calculated heat flow for the ensenada region, baja california, mexico. *Ciencias Marinas* 27 (4), 619–634, doi:10.7773/cm.v27i4.497.
- Blackwell, D. D., Negraru, P. T., Richards, M. C., Dec. 2006. Assessment of the Enhanced Geothermal System Resource Base of the United States. *Natural Resources Research* 15 (4), 283–308, doi:10.1007/s11053-007-9028-7.
- Blackwell, D. D., Richards, M. C., 2004. Geothermal map of North America: Scale 1:6,500,000. Am. Assoc. Petrol. Geol., product Code 423.
- Blatter, D. L., Hammersley, L., 2010. Impact of the Orozco Fracture Zone on the central Mexican Volcanic Belt. *Journal of Volcanology and Geothermal Research* 197 (1), 67–84, doi:10.1016/j.jvolgeores.2009.08.002.
- Bonham-Carter, G. F., 1994. Geographic Information Systems for Geoscientists: Modelling with GIS. Elsevier, Canada, google-Books-ID: FkKe-BQAAQBAJ.
- Bouligand, C., Glen, J. M. G., Blakely, R. J., 2009. Mapping Curie temperature depth in the western United States with a fractal model for crustal magnetization. *Journal of Geophysical Research: Solid Earth* 114 (B11), doi:10.1029/2009JB006494.
- Brunsdon, C., Comber, L., 2015. An Introduction to R for Spatial Analysis and Mapping. SAGE, google-Books-ID: ViCJCwAAQBAJ.
- Campa, M. F., Coney, P. J., Jun. 1983. Tectono-stratigraphic terranes and mineral resource distributions in Mexico. *Canadian Journal of Earth Sciences* 20 (6), 1040–1051, doi:10.1139/e83-094.
- Campos-Enriquez, J. O., Arroyo-Esquivel, M. A., Urrutia-Fucugauchi, J., Jan. 1990. Basement, Curie isotherm and shallow-crustal structure of the Trans-Mexican Volcanic Belt, from aeromagnetic data. *Tectonophysics* 172 (1), 77–90, doi:10.1016/0040-1951(90)90060-L.
- Chang, K.T., 2004. Introduction to geographic information systems, 2nd Edition. McGraw-Hill.
- Cull, J., Sparksman, G., 1977. Measurements of Surface Heat Flow. Bureau of Mineral Resources Geology and Geophysics Record 12 (39), 1–17.
- Davies, J. H., 2013. Global map of solid Earth surface heat flow. *Geochemistry, Geophysics, Geosystems* 14 (10), 4608–4622, doi:10.1002/ggge.20271.
- Davies, J. H., Davies, D. R., 2010. Earth's surface heat flux. *Solid Earth* 1 (1), 5–24, doi:10.5194/se-1-5-2010.
- De Anda, L. F., Septien, J. I., Elizondo, J. R., 1964. Geothermal energy in Mexico. Proceedings of the UN Conference on New Sources of Energy 2, 149–165, new York; United Nations.
- Eguiluz-de Antuñano, S., 2009. The Yegua Formation: Gas Play in the Burgos Basin, Mexico, in C. Bartolini, and J. R. Roman Ramos, eds., Petroleum systems in the southern Gulf of Mexico: American Association of Petroleum Geologist Memoir 90, 49–77, doi:10.1306/13191077M902621.
- Epp, D., Gnim, P. J., Langseth, M. G., Oct. 1970. Heat flow in the Caribbean and Gulf of Mexico. *Journal of Geophysical Research* 75 (29), 5655–5669, doi:10.1029/JB075i029p05655.
- Espinosa-Cerdeña, J. M., Campos-Enriquez, J. O., Oct. 2008. Curie point depth from spectral analysis of aeromagnetic data from Cerro Prieto geothermal area, Baja California, México. *Journal of Volcanology and Geothermal Research* 176 (4), 601–609, doi:10.1016/j.jvolgeores.2008.04.014.
- Espinosa-Ojeda, O. M., Prol-Ledesma, R. M., Iglesias, E. R., 2017a. Continental heat flow data update for México – Constructing a reliable and accurate heat flow map, in Proceedings of the 42nd Workshop on Geothermal Reservoir Engineering 2017: Stanford, California, USA, 13–15 February 2017SGP-TR-212.
- Espinosa-Ojeda, O. M., Prol-Ledesma, R. M., Iglesias, E. R., Figueroa-Soto, A., 2017b. Update and review of heat flow measurements in México. *Energy* 121, 466–479, doi:10.1016/j.energy.2017.01.045.
- Ferrari, L., Tagami, T., Eguchi, M., Orozco-Esquivel, M. T., Petrone, C. M., Jacobo-Albarrán, J., López-Martínez, M., 2005. Geology, geochronology and tectonic setting of late Cenozoic volcanism along the southwestern Gulf of Mexico: The Eastern Alkaline Province revisited. *Journal of Volcanology and Geothermal Research* 146 (4), 284–306, doi:10.1016/j.jvolgeores.2005.02.004.
- Ferrari, L., Valencia-Moreno, M., Bryan, S., 2007. Magmatism and tectonics of the Sierra Madre Occidental and its relation with the evolution of the western margin of North America. In: Special Paper 422: Geology of México: Celebrating the Centenary of the Geological Society of México. Vol. 422. Geological Society of America, pp. 1–39, doi:10.1130/2007.2422(01).
- Fisher, A. T., Giambalvo, E., Sclater, J., Kastner, M., Ransom, B., Weinstein, Y., Lonsdale, P., 2001. Heat flow, sediment and pore fluid chemistry, and hydrothermal circulation on the east flank of Alarcon Ridge, Gulf of California. *Earth and Planetary Science Letters* 188 (3), 521–534, doi:10.1016/S0012-821X(01)00310-7.
- Flores-Márquez, E.L., Chávez-Segura, R., Campos-Enríquez, O., Pilkington, M., 1999. Preliminary 3-D structural model from the Chicxulub impact crater and its implications in the actual geothermal regime. *Trends in Heat, Mass and Momentum Transfer* 5, 19–40.
- García-Estrada, G., 2000. Modelado del estado térmico inicial del campo geotérmico de Los Azufres, Michoacán, México. PhD Thesis. Universidad Nacional Autónoma de México, Posgrado en Ciencias de la Tierra, UNAM, http://132.248.9.195/pd2000/285393/Index.html.
- Goutorbe, B., Poort, J., Lucaleau, F., Raillard, S., 2011. Global heat flow trends resolved from multiple geological and geophysical proxies. *Geophysical Journal International* 187 (3), 1405–1419, doi:10.1111/j.1365-246X.2011.05228.x.
- Iglesias, E.R., Torres, R.J., Martínez-Estrella, J.I., Reyes-Picasso, N., 2015. Summary of the 2014 Assessment of Medium- to Low-Temperature Mexican Geothermal Resources. In World Geothermal Congress, 16–24 April 2015, Australia-New Zealand: proceedingsPaper 16081, 7pp.
- Instituto Nacional de Estadística, Geografía e Informática (INEGI), 2001. Conjunto de datos vectoriales Fisiográficos. Continuo Nacional escala 1:1,000,000 serie I. Provincias fisiográficas. INEGI, http://www.beta.inegi.org.mx/temas/mapas/fisiografia/.
- Japan International Cooperation Agency (JICA), 1989. Evaluación del yacimiento geotérmico en La Primavera. JICA, 122 pp.
- Jácome-Paz, M.P., Pérez-Zárate, D., Prol-Ledesma, R.M., Rodríguez-Díaz, A.A., Estrada-Murillo, A.M., González-Romo, I. A., Magaña-Torres, E., 2018. Two new geothermal prospects in the Mexican Volcanic Belt: La Escalera and Agua Caliente–Tzitzio geothermal springs, Michoacán, México(submitted).
- Khutorskoy, M. D., Fernandez, R., Kononov, V. I., Polyak, B. G., Matveev, V. G., Rot, A. A., 1990. Heat flow through the sea bottom around the Yucatan Peninsula. *Journal of Geophysical Research: Solid Earth* 95 (B2), 1223–1237, doi:10.1029/JB095iB02p01223.
- Lawver, L. A., Williams, D. L., 1979. Heat flow in the central Gulf of California. *Journal of Geophysical Research: Solid Earth* 84 (B7), 3465–3478, doi:10.1029/JB084iB07p03465.
- Lippmann, M. J., Truesdell, A. H., Halfman-Dooley, S. E., A., M., 1991. A review of the hydrogeologic-geochemical model for Cerro Prieto. *Geothermics* 20 (1-2), 39–52, doi:10.1016/0375-6505(91)90004-F.
- Manea, M., Manea, V. C., 2010. Curie Point Depth Estimates and Correlation with Subduction in Mexico. *Pure and Applied Geophysics* 168 (8), 1489–1499, doi:10.1007/s00024-010-0238-2.
- Marvin, P.R., 1984. Regional heat flow based on the silica content of ground waters from northcentral Mexico. M.Sc. Thesis. New Mex. St. Univ., 107 p.
- Moeck, I., Beardmore, G., 2014. A New 'Geothermal Play Type' Catalog: Streamlining Exploration Decision Making. Proceedings. Thirty-Ninth Workshop on Geothermal Reservoir EngineeringStanford, California: Stanford University; p. 8.
- Morán-Zenteno, D., 1986. Breve revisión sobre la evolución tectónica de México. *Geofísica Internacional* 25 (1), 9–38.
- Morán-Zenteno, D.J., Cerca, M., Keppie, J.D., 2007. The Cenozoic tectonic and magmatic evolution of southwestern México: Advances and problems of interpretation, in Alaniz-Álvarez, S.A. & Nieto-Samaniego, Á.F., eds., Geology of México: Celebrating the Centenary of the Geological Society of México. Geological Society of America Special Paper 422, 71–91, doi:10.1130/2007.2422(03).
- Muffler, P., 1979. Assessment of geothermal resources of the United States—1978. U.S.G.S. Circular 790.
- Muffler, P., Cataldi, R., 1978. Methods for regional assessment of geothermal resources. *Geothermics* 7 (2), 53–89, doi:10.1016/0375-6505(78)90002-0.
- Nagihara, S., Sclater, J. G., Phillips, J. D., Behrens, E. W., Lewis, T., Lawver, L. A., Nakamura, Y., Garcia-Abdeslem, J., Maxwell, A. E., 1996. Heat flow in the western abyssal plain of the Gulf of Mexico: Implications for thermal evolution of the old oceanic lithosphere. *Journal of Geophysical Research* 101 (B2), 2895–2913, doi:10.1029/95JB03450.
- Neumann, F., Negrete-Aranda, R., Harris, R. N., Contreras, J., Sclater, J. G., González-Fernández, A., Dec. 2017. Systematic heat flow measurements

- across the Wagner Basin, northern Gulf of California. *Earth and Planetary Science Letters* 479, 340–353, doi:10.1016/j.epsl.2017.09.037.
- Norton, D., Knight, J. E., 1977. Transport phenomena in hydrothermal systems; cooling plutons. *American Journal of Science* 277 (8), 937–981, doi:10.2475/ajs.277.8.937.
- Okubo, Y., Graf, R., Hansen, R., Ogawa, K., Tsu, H., 1985. Curie point depths of the Island of Kyushu and surrounding areas, Japan. *GEOPHYSICS* 50 (3), 481–494, doi:10.1190/1.1441926.
- Okubo, Y., Tsu, H., Ogawa, K., 1989. Estimation of Curie point temperature and geothermal structure of island arcs of Japan. *Tectonophysics* 159 (3), 279–290, doi:10.1016/0040-1951(89)90134-0.
- Padilla y Sánchez, R., Domínguez Trejo, I., López Azcárraga, A., Mota Nieto, J., Fuentes Menes, A., Rosique Naranjo, F., Germán Castelán, E., Campos Arriola, S., 2013. National Autonomous University of Mexico Tectonic Map of Mexico GIS Project, American Association of Petroleum Geologists GIS Open Files series.
- Polyak, B. G., 2005. Heat and mass transfer from the mantle: heat flow and He-isotope constraints. *Annals of Geophysics* 48 (1), 9–17.
- Polyak, B. G., Kononov, V. I., Kamensky, I., Prasolov, E. M., Sharkov, I. V., Prol-Ledesma, R. M., Gonzalez, A., Razo, A., Molina-Berbeller, R., 1985. First estimations of terrestrial heat flow in the TMVB and adjacent areas based on isotopic composition of natural helium. *Geofísica Internacional* 24 (4), 465–476.
- Polyak, B. G., Tolstikhin, I. N., 1985. Isotopic composition of the earth's helium and the problem of the motive forces of tectogenesis. *Chemical Geology: Isotope Geoscience section* 52 (1), 9–33, doi:10.1016/0168-9622(85)90005-3.
- Prol-Ledesma, R. M., 1990. Mapa geotérmico de la República Mexicana. Atlas Nacional de México. Vol. 3. Instituto de Geografía, UNAM.
- Prol-Ledesma, R. M., 1991a. Chemical geothermometers applied to the study of thermalized aquifers in Guaymas, Sonora, Mexico: a case history. *Journal of Volcanology and Geothermal Research* 46 (1), 49–59, doi:10.1016/0377-0273(91)90075-B.
- Prol-Ledesma, R. M., 1991b. Terrestrial Heat Flow in Mexico. In: Čermák, V., Rybach, L. (Eds.), *Terrestrial Heat Flow and the Lithosphere Structure. Exploration of the Deep Continental Crust*. Springer Berlin Heidelberg, Berlin, Heidelberg, pp. 475–485, doi:10.1007/978-3-642-75582-8_24.
- Prol-Ledesma, R. M., 2018. Anomalías de flujo de calor terrestre y la definición de la provincia geotérmica asociada al volcanismo de intraplaca en México. Trabajo de Ingreso a la Academia de Ingeniería México. [Http://www.ai.org.mx/presentacion/anomalias-de-flujo-de-calor-terrestre-y-la-definicion-de-la-provincia-geotermica](http://www.ai.org.mx/presentacion/anomalias-de-flujo-de-calor-terrestre-y-la-definicion-de-la-provincia-geotermica).
- Prol-Ledesma, R. M., Arango-Galván, C., 2017. Sistemas Geotérmicos de la Península de Baja California. Vol. 21. Monografías del Instituto de Geofísica, UNAM, 233 pp.
- Prol-Ledesma, R. M., Espinoza-Ojeda, O.M., Iglesias, E.R., Arango-Galván, C., 2016. Integration of heat flow measurements and estimations in the construction of Mexico's heat flow map. *Proceedings European Geothermal Congress 2016* Strasbourg, France, 19–24 Sept.
- Prol-Ledesma, R. M., Juarez, G., 1986. Geothermal map of Mexico. *Journal of Volcanology and Geothermal Research* 28 (3), 351–362, doi:10.1016/0377-0273(86)90030-2.
- Prol-Ledesma, R. M., Sugrobov, V. M., Flores, E. L., Juárez M., G., Smirnov, Y. B., Gorshkov, A. P., Bondarenko, V. G., Rashidov, V. A., Nedopekin, L. N., Gavrilov, V. A., 1989. Heat flow variations along the Middle America Trench. *Marine Geophysical Researches* 11 (1), 69–76, doi:10.1007/BF00286248.
- Prol-Ledesma, R. M., Torres-Vera, M. A., 2007. Mapa de Recursos Geotérmicos de la República Mexicana. Atlas Nacional de México. Instituto de Geografía, UNAM. E-VI-3.
- Prol-Ledesma, R. M., Torres-Vera, M.-A., Rodolfo-Metalpa, R., Ángeles, C., Lechuga Devezé, C. H., Villanueva-Estrada, R. E., Shumilin, E., Robinson, C., 2013. High heat flow and ocean acidification at a nascent rift in the northern Gulf of California. *Nature Communications* 4, 1388, doi:10.1038/ncomms2390.
- Reiter, M., Tovar R., J. C., 1982. Estimates of terrestrial heat flow in northern Chihuahua, Mexico, based upon petroleum bottom-hole temperatures. *GSA Bulletin* 93 (7), 613–624, doi:10.1130/0016-7606(1982)93<613:EOTHFI>2.0.CO;2.
- Richards, M., Blackwell, D., Williams, M., Frone, Z., Dingwall, R., Batir, J., Chickering, C., 2012. Proposed Reliability Code for Heat Flow Sites. *GRC Transactions* 36.
- Sedlock, R.L., Ortega-Gutiérrez, F., Speed, C., 1993. Tectonostratigraphic Terranes and Tectonic Evolution of Mexico. *Geological Society of America Special Paper* 278, 153 p. doi:10.1130/SPE278-p1.
- Setianto, A., Triandini, T., 2013. COMPARISON OF KRIGING AND INVERSE DISTANCE WEIGHTED (IDW) INTERPOLATION METHODS IN LINEAMENT EXTRACTION AND ANALYSIS. *Journal of Applied Geology* 5 (1), 21–29, doi:10.22146/jag.7204.
- Shepard, D., 1968. A two-dimensional interpolation function for irregularly-spaced data. *Proceedings of the 1968 ACM National Conference*, 517–524. doi:10.1145/800186.810616.
- Smith, D. L., 1974. Heat flow, radioactive heat generation, and theoretical tectonics for northwestern Mexico. *Earth and Planetary Science Letters* 23 (1), 43–52, doi:10.1016/0012-821X(74)90028-4.
- Smith, D. L., Nuckles, C. E., Jones, R. L., Cook, G. A., 1979. Distribution of heat flow and radioactive heat generation in northern Mexico. *Journal of Geophysical Research: Solid Earth* 84 (B5), 2371–2379, doi:10.1029/JB084iB05p02371.
- Swanberg, C. A., Morgan, P., 1978. The linear relation between temperatures based on the silica content of groundwater and regional heat flow: A new heat flow map of the United States. *Pure and Applied Geophysics* 117 (1), 227–241, doi:10.1007/BF00879749.
- Swanberg, C. A., Morgan, P., 1980. The silica heat flow interpretation technique: Assumptions and applications. *Journal of Geophysical Research: Solid Earth* 85 (B12), 7206–7214, doi:10.1029/JB085iB12p07206.
- Vacquier, V., Slater, J.G., Corry, C.F., 1967. Studies of the thermal state of the Earth. 21st paper. *Heat Flow, Eastern Pacific*, 45, 375–393.
- Van Wees, J.D., Boxem, T., Calcagno, P., Dezayes, C., Lacasse, C., Manzella, A., 2013. A Methodology for Resource assessment and application to core countries. Deliverable no. 2.1 (final). GEO-ELEC project, 28 pp.
- Vidal-Solano, J.R., Paz Moreno, F.A., Demant, A., 2005. Caracterización y Cronología del Evento Volcánico Terciario Pre-Pinacate, Campo El Pinacate, Noroeste de Sonora, Mexico. *Bol. Depto. Geol. UniSon* 18–19, 117–140.
- Von Herzen, R. P., 1963. Geothermal Heat Flow in the Gulfs of California and Aden. *Science* 140 (3572), 1207–1208, doi:10.1126/science.140.3572.1207.
- Von Herzen, R. P., Uyeda, S., 1963. Heat flow through the eastern Pacific ocean floor. *Journal of Geophysical Research* 68 (14), 4219–4250, doi:10.1029/JZ068i014p04219.
- Wang, F., 2006. Quantitative Methods and Applications in GIS. CRC Press, doi:10.1201/9781420004281.
- White, D. E., Williams, D. L., 1975. Assessment of geothermal resources of the United States—1975. *U.S. Geological Survey Circular* 726, 155 p.
- Wilhelm, H., Heidinger, P., Safanda, J., Čermák, V., Burkhardt, H., Popov, Y., 2004. High resolution temperature measurements in the borehole Yaxcopoil-1, Mexico. *Meteoritics & Planetary Science* 39, 813–819. doi:10.1111/j.1945-5100.2004.tb00931.x.
- Ziajas, J. P., Blackwell, D. D., Mooser, F., 1985. Heat flow in southern Mexico and the thermal effects of subduction. *Journal of Geophysical Research: Solid Earth* 90 (B7), 5410–5420, doi:10.1029/JB090iB07p05410.

This article accompanies the following material:

HTML:	DOI: 10.22201/igg.25940694.2018.2.51.103
Static map:	DOI: 10.22201/igg.25940694.2018.2.51.104

Appendix

Appendix Table 1. Data table (unpublished)

New and revised heat flow data are included in Table 1. We used published temperature logs and BHT (a – García-Estrada, 2000; b – De Anda et al., 1964; c – Prol-Ledesma, 1991a; d – JICA, 1989; e – Lippmann et al., 1991 ; f – Espinoza-Ojeda et al., 2017; g – Wilhelm et al., 2004) as well as temperature data measured by our group to calculate the geothermal gradient. Heat flow was calculated following the methodology explained in this paper. Thermal conductivity was estimated based on lithology, and when lithology was not reported for the well, we assigned the crust average conductivity value (2.5 W/m °K). All new and recalculated data presented in Table 1 were included in the heat flow map produced here. The columns of the table include: data number, original site ID, temperature data source (reference), site location in geographic coordinates, calculated geothermal gradient (°C/km), conductivity (W/m °K; estimated from lithology or average crust value “*”), heat flow (mW/m²).

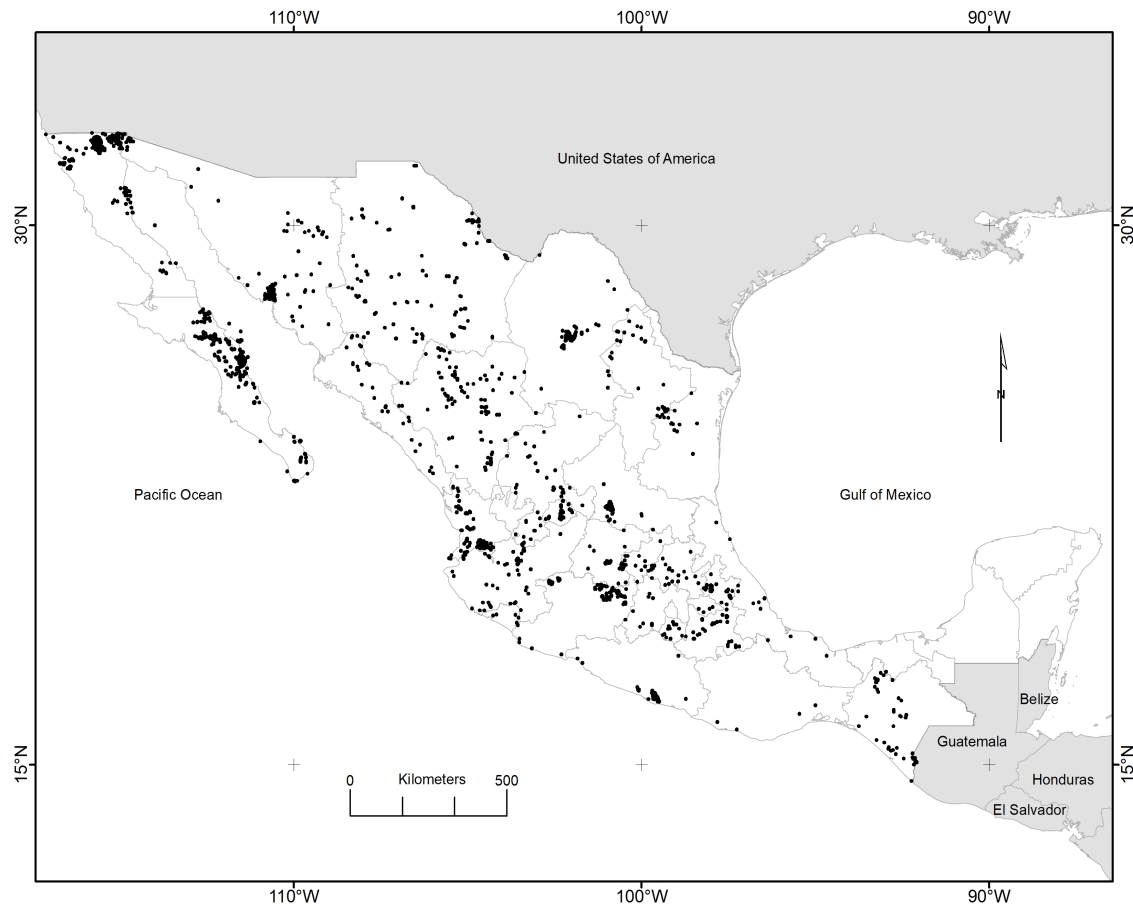
Appendix Table 1. New heat flow data produced by temperature gradient measurement (Grad-T-this work); temperature gradient from references (Grad-T-a,b,...) and recalculation of heat flow data with additional information (Rec-f). Thermal conductivity based on well lithology or crustal average (*) / Tabla 1 del apéndice. Nuevos datos de flujo de calor producidos a partir de mediciones de gradiente de temperatura (Grad-T- este trabajo); gradiente de temperatura de referencias (Grad-T-a,b,...) y nuevos cálculos de datos de flujo de calor con información adicional (Rec-f). La conductividad térmica se tomó de la litología del pozo o bien del valor promedio de la corteza(*).

Data #	Data production	Site ID	Long.	Lat.	Depth (m)	Geoth. Grad. (C/Km)	Conductivity (W/mK)	Heat Flow (mW/m ²)
1	Grad-T-this work	Fraile 1	-101.33430	25.02550	334	20.0	2.50*	50.1
2	Grad-T-this work	Difuntita	-101.19090	25.06305	509	28.5	2.50*	71.2
3	Grad-T-this work	Texcoco	-98.84960	19.50729	337	29.4	2.50*	73.6
4	Grad-T-a	1	-100.66489	19.79216	2159	139.7	1.87	261.3
5	Grad-T-a	3	-100.68695	19.80533	2440	99.3	1.84	182.3
6	Grad-T-a	12	-100.67013	19.79218	898	256.6	1.87	479.8
7	Grad-T-a	16	-100.67021	19.77975	2500	132.7	1.87	248.1
8	Grad-T-a	18	-100.65425	19.78473	1324	214.4	1.87	401.0
9	Grad-T-a	19	-100.66752	19.82438	1663	154.8	1.87	289.4
10	Grad-T-a	21	-100.67644	19.82662	1705	153.7	1.87	287.4
11	Grad-T-a	22	-100.66094	19.78968	1246	215.5	2.17	467.6
12	Grad-T-a	23	-100.67494	19.79773	1729	141.8	1.87	265.1
13	Grad-T-a	25	-100.66305	19.79787	1600	182.2	1.75	318.9
14	Grad-T-a	26	-100.65038	19.79787	1240	201.8	1.77	356.5
15	Grad-T-a	31	-100.64631	19.78205	1295	221.6	1.87	414.4
16	Grad-T-a	34	-100.65916	19.78459	860	292.6	1.87	547.2
17	Grad-T-a	35	-100.65424	19.79059	1225	220.4	1.87	412.1
18	Grad-T-a	37	-100.67064	19.78603	859	241.7	1.87	452.0
19	Grad-T-a	43	-100.65931	19.82277	1500	185.6	1.87	347.0
20	Grad-T-a	44	-100.68244	19.82122	2440	88.7	1.87	165.9
21	Grad-T-a	46	-100.66807	19.78246	970	258.0	1.87	482.4
22	Grad-T-a	47	-100.66438	19.78621	2957	102.9	1.89	194.5
23	Grad-T-a	48	-100.66403	19.82548	2669	93.2	1.87	174.3
24	Grad-T-a	49	-100.65831	19.81669	2400	126.1	1.87	235.9
25	Grad-T-a	51	-100.66252	19.83178	1842	158.9	1.87	297.1
26	Grad-T-a	53	-100.66228	19.82938	1201	201.0	1.87	375.8
27	Grad-T-a	54	-100.68695	19.81525	898	211.2	1.87	395.0
28	Grad-T-a	55	-100.65800	19.78985	1403	206.1	1.87	385.4
29	Grad-T-a	56	-100.67200	19.81009	2305	113.2	1.87	211.7
30	Grad-T-a	57	-100.67038	19.82422	1722	156.8	1.87	293.3
31	Grad-T-a	E1	-100.72993	19.82779	1995	94.8	1.87	177.3
32	Grad-T-a	E2	-100.71824	19.80483	1992	106.5	1.87	199.2
33	Grad-T-b	Pozo No. 4	-99.69570	20.56765	372	161.3	2.43	392.0
34	Grad-T-b	Pozo No. 5	-99.68648	20.57404	460	144.4	2.43	351.0
35	Grad-T-c	1	-110.67043	28.05821	90	28.7	2.50*	71.7
36	Grad-T-c	2	-110.70826	28.01467	71	89.5	2.50*	223.8
37	Grad-T-c	3	-110.68684	28.10318	109	79.0	2.50*	197.5
38	Grad-T-c	4	-110.67828	28.17314	136	101.4	2.50*	253.5
39	Grad-T-c	5	-110.69827	27.94543	124	41.7	2.50*	104.2
40	Grad-T-c	6	-110.61832	28.34803	147	197.4	2.50*	493.4

41	Grad-T-c	7	-110.73610	28.09105	98	49.7	2.50*	124.2
42	Grad-T-c	8	-110.77607	28.02966	61	94.6	2.50*	236.6
43	Grad-T-c	9	-110.74538	28.01253	89	36.0	2.50*	90.1
44	Grad-T-c	10	-110.67899	28.14601	149	103.1	2.50*	257.8
45	Grad-T-d	PR2	-103.53115	20.66423	1988	114.9	2.17	249.3
46	Grad-T-d	PR8	-103.52068	20.66012	1855	137.3	2.24	307.5
47	Grad-T-d	PR10	-103.51935	20.66183	2086	107.0	1.99	213.0
48	Grad-T-d	PR11	-103.52418	20.65634	2125	77.7	2.24	174.1
49	Grad-T-e	M203	-115.18686	32.39283	3958	114.4	2.42	277.0
50	Rec-f	MEX001	-115.34450	32.44840	1825	18.0	2.86	51.5
51	Rec-f	MEX002	-115.34500	32.43200	2200	11.7	2.50*	29.3
52	Rec-f	MEX003	-111.41250	26.25000	500	12.5	2.55	31.9
53	Rec-f	MEX004	-111.53500	26.24000	500	50.8	2.50*	126.9
54	Rec-f	MEX006	-103.52694	20.29167	1950	29.1	2.50*	72.8
55	Rec-f	MEX007	-103.53333	20.32278	800	49.4	2.07	102.0
56	Rec-f	MEX010	-103.51889	20.65639	2271	125.6	2.12	266.3
57	Rec-f	MEX011	-104.69500	21.11667	1911	102.5	2.50	256.3
58	Rec-f	MEX012	-104.72917	21.08333	200	53.2	2.50*	133.0
59	Rec-f	MEX013	-104.71667	21.10000	430	103.6	2.50*	259.0
60	Rec-f	MEX014	-104.54942	21.09294	2801	29.2	2.32	67.5
61	Rec-f	MEX015	-104.70167	21.18750	1911	52.4	3.05	159.7
62	Rec-f	MEX017	-112.55622	27.50772	2500	69.0	2.48	171.3
63	Rec-f	MEX018	-112.55890	27.50643	2505	94.6	2.37	224.3
64	Rec-f	MEX019	-112.53444	27.49995	1250	133.8	2.33	311.9
65	Rec-f	MEX022	-97.45561	19.66426	1810	203.0	2.09	424.0
66	Rec-f	MEX023	-97.44878	19.64046	2300	74.0	3.14	232.4
67	Rec-f	MEX024	-97.46761	19.69002	1670	230.8	2.10	484.6
68	Rec-f	MEX025	-97.45516	19.68642	1880	90.8	2.08	188.5
69	Rec-f	MEX027	-97.45619	19.67156	2310	152.7	2.22	338.8
70	Rec-f	MEX028	-97.45859	19.67629	2350	141.5	2.09	295.4
71	Rec-f	MEX030	-97.45383	19.67615	2160	123.6	2.20	272.4
72	Rec-f	MEX031	-97.44904	19.68564	2480	212.0	2.17	459.5
73	Rec-f	MEX032	-97.43770	19.64594	3100	165.9	2.41	399.4
74	Rec-f	MEX036	-97.45157	19.69623	2265	164.8	2.15	354.1
75	Rec-f	MEX037	-97.42717	19.63703	2903	98.5	2.14	210.7
76	Rec-f	MEX038	-97.44618	19.67845	2292	225.7	2.20	496.6
77	Rec-f	MEX039	-97.44182	19.68603	2402	236.6	2.12	501.5
78	Rec-f	MEX040	-97.45165	19.70603	2220	134.3	2.28	305.8
79	Rec-f	MEX041	-97.47294	19.69864	1500	189.6	2.56	485.8
80	Rec-f	MEX042	-97.43386	19.66764	2620	167.6	2.30	385.5
81	Rec-f	MEX043	-97.42156	19.64476	3270	109.7	2.23	245.1
82	Rec-f	MEX044	-97.44875	19.68839	2577	155.7	2.19	341.4
83	Rec-f	MEX045	-97.45558	19.68937	2200	120.5	2.43	293.2
84	Rec-f	MEX047	-97.45598	19.70020	1926	173.3	2.13	369.8
85	Rec-f	MEX048	-97.44844	19.69112	2200	162.3	2.09	339.9
86	Rec-f	MEX050	-97.44533	19.68354	1800	209.3	2.21	462.4
87	Rec-f	MEX051	-97.46339	19.69418	1700	234.6	2.20	515.5
88	Rec-f	MEX052	-97.44914	19.68528	1800	216.7	2.04	442.7
89	Rec-f	MEX055	-97.44185	19.64813	2500	84.3	2.21	186.2
90	Rec-f	MEX057	-97.43990	19.64801	2200	173.1	2.11	364.8
91	Rec-f	MEX058	-97.44226	19.65002	2200	184.4	2.17	400.5
92	Rec-f	MEX059	-97.46233	19.69116	2200	192.2	2.57	493.3
93	Rec-f	MEX060	-98.14294	19.92120	2000	143.5	2.98	426.8
94	Rec-f	MEX061	-98.13815	19.92339	1900	107.2	2.46	263.2
95	Rec-f	MEX064	-113.02362	25.98614	2244	25.1	2.19	55.0
96	Rec-f	MEX065	-111.84375	25.37281	3014	26.1	2.45	63.9
97	Rec-f	MEX066	-111.92245	24.88475	2500	32.4	2.36	76.5
98	Rec-f	MEX067	-111.72009	24.89025	2657	29.3	2.66	77.9
99	Rec-f	MEX068	-113.73551	27.65183	2405	34.9	1.90	66.3
100	Rec-f	MEX069	-114.88719	28.29299	2811	28.1	2.50*	70.3
101	Rec-f	MEX071	-111.88591	25.70630	3300	17.9	2.21	39.4

102	Rec-f	MEX072	-113.71727	27.63163	2325	37.1	2.36	87.7
103	Rec-f	MEX073	-114.51855	30.51737	3191	41.7	2.25	93.7
104	Rec-f	MEX074	-113.91369	27.92988	3298	30.2	2.45	74.1
105	Rec-f	MEX075	-115.03122	32.29032	3843	52.8	2.41	127.1
106	Rec-f	MEX076	-114.23769	31.38266	4799	29.9	2.57	76.7
107	Rec-f	MEX077	-114.27832	31.34619	3302	25.1	2.50*	62.7
108	Rec-f	MEX078	-114.21425	31.37561	3300	27.1	2.50*	67.7
109	Rec-f	MEX079	-113.87737	28.00498	1944	25.0	2.27	56.8
110	Rec-f	MEX080	-113.40627	27.50679	3000	19.5	2.26	44.1
111	Rec-f	MEX081	-113.84537	27.96591	2503	32.7	2.44	79.7
112	Rec-f	MEX082	-114.19665	30.83823	4930	51.3	2.50*	128.2
113	Rec-f	MEX083	-113.70833	27.51782	1363	41.8	2.48	103.7
114	Rec-f	MEX084	-113.38321	27.06762	4600	25.8	2.50*	64.5
115	Rec-f	MEX086	-111.83968	25.37540	4424	17.4	2.22	38.5
116	Rec-f	MEX087	-112.43983	25.76848	4505	25.6	2.19	56.0
117	Rec-f	MEX088	-111.98696	25.07088	3762	33.4	2.11	70.4
118	Rec-f	MEX089	-113.72808	27.58101	2750	34.3	2.29	78.6
119	Rec-f	MEX090	-114.09778	31.29304	3302	31.6	2.63	83.0
120	Rec-f	MEX091	-113.88876	31.11501	4340	47.3	2.23	105.7
121	Rec-f	MEX092	-113.79516	27.68947	3270	19.6	2.50*	49.1
122	Rec-f	MEX093	-113.18670	27.10718	3002	55.4	2.50*	138.6
123	Rec-f	MEX094	-112.87839	29.63975	4813	59.6	2.50*	149.1
124	Rec-f	MEX095	-113.75645	27.66715	2985	30.8	2.50*	77.0
125	Rec-f	MEX096	-113.90057	27.95947	2636	31.5	2.50*	78.8
126	Rec-f	MEX097	-114.65351	28.39972	4450	28.6	2.50*	71.5
127	Rec-f	MEX098	-114.76003	32.37662	2918	29.9	2.57	76.9
128	Rec-f	MEX099	-114.19423	31.26245	5591	23.3	2.47	57.4
129	Rec-f	MEX100	-110.25876	27.18580	2471	30.7	2.36	72.5
130	Rec-f	MEX101	-114.61628	31.80176	5325	27.2	2.49	67.7
131	Rec-f	MEX102	-114.94561	32.00882	4530	35.0	2.55	89.1
132	Rec-f	MEX103	-114.36411	31.62076	3872	33.3	2.50*	83.3
133	Rec-f	MEX104	-114.75972	32.00861	5152	44.1	2.50*	110.3
134	Rec-f	MEX105	-114.38430	31.79458	3887	29.4	2.42	71.2
135	Rec-f	MEX106	-104.73863	28.88995	6509	31.9	2.24	71.3
136	Rec-f	MEX107	-105.02839	28.46334	3903	30.2	2.16	65.2
137	Rec-f	MEX108	-100.97323	27.42872	3038	35.4	3.18	112.7
138	Rec-g	UNAM-5	-89.77927	20.38739	335	24.8	2.00	49.5

Appendix Figure 1



Appendix Figure 1. Map of hydrothermal manifestations in Mexico. (After: Iglesias et al., 2015; Prol-Ledesma & Arango-Galván, 2017) / Figura 1 del apéndice.
Mapa de las manifestaciones hidrotermales en México.